Phonon thermal transport in transition-metal and rare-earth nitride semiconductors from first principles

Chunhua Li and David Broido

Phys. Rev. B **95**, 205203 — Published 22 May 2017

DOI: 10.1103/PhysRevB.95.205203

Phonon thermal transport in transition metal and rare earth nitride semiconductors from first principles

Chunhua Li and David Broido

Department of Physics, Boston College, Chestnut Hill, MA 02467 USA

Abstract

The thermal properties of three transition metal and rare earth nitride compounds, ScN, YN and LuN, have been studied using a first principles approach, in which a DFT+U treatment is guided by accurate hybrid functional calculations of electronic structure. The phonon dispersions for the three compounds show large LO-TO splitting and soft TO modes. The resulting strong anharmonic scattering between acoustic and TO phonons reduces the lattice thermal conductivities, κ_L, of these compounds. The room temperature κ_L values of YN and LuN are more than an order of magnitude smaller than that found for the weakly polar III-V compound boron bismuth (350 $Wm^{-1}K^{-1}$), in spite of the latter having much larger average atomic mass and smaller acoustic phonon velocities. This work demonstrates the utility of first principles calculations in understanding the thermal properties of materials, and it highlights the importance of optic phonons in reducing κ_L.

PACS: 66.70.-f, 63.20.kg, 71.15.Mb, 31.15.E-

I. Introduction

There has been considerable interest recently in the properties of transition metal (TM) and rare earth (RE) mononitrides [1–3], such as high melting points, mechanical strength and hardness. Yet, to date little attention has been devoted to understanding thermal transport in these compounds. Most TM and RE based binary compounds are metallic. Here we examine thermal transport in three semiconducting binary nitride compounds containing TM and RE atoms: ScN, YN and LuN. Under ambient conditions all three compounds crystallize in the rock-salt structure. There has been disagreement in the literature regarding whether these compounds are metallic or semiconducting. For example, electronic structure calculations based on density functional theory (DFT) have found ScN and YN to be metallic [4, 5]. However, the authors of Ref. [6] argued that they should be semiconducting based on the fact that the three *s* and *d* electrons from the metal atom combine with the five valence electrons from the nitrogen atom to give a closed shell. The semiconducting behavior for all three compounds has been confirmed through accurate screened exchange, hybrid functional DFT, and GW calculations [2,5,6, 8–10], with experimental confirmation for ScN [5, 11].

For intrinsic semiconductors, thermal transport is dominated by phonons. Here, we present first principles calculations of the intrinsic lattice thermal conductivity κ_L, for ScN, YN and LuN, which is limited only by three-phonon scattering that arises from the anharmonicity of the interatomic potential [12]. This gives an upper bound to the thermal conductivities of real crystals, in which phonons can also scatter from extrinsic defects such as point impurities, and from boundaries. The phonon spectra show stiff bonding reflected in the high phonon frequency scales and large acoustic phonon velocities comparable to those seen in group IV and III-V semiconductors, such as SiC and GaN. However, unlike the group IV and III-V compounds, the

three TM and RE nitride compounds show a strong polar nature seen in large frequency splittings between the longitudinal optic (LO) and transverse optic (TO) phonon branches. All compounds also show soft TO phonon modes around the Γ point. These features promote strong phonon-phonon scattering that suppresses the lattice thermal conductivities in these compounds.

In section II, the first principles theory used to calculate phonon thermal transport and lattice thermal conductivity is presented. Section III gives a description of the computational details, section IV discusses the results, and section V presents a summary and conclusions.

II. Theory

We have confirmed the previous finding that ScN, YN and LuN are semiconductors by performing electronic structure calculations using the screened hybrid functional of Heyd, Scuseria and Ernzerhof (HSE06) [13] within density functional theory. The band structure along some high symmetry directions is presented in Figs. 1 (a)–(c) for ScN, YN and LuN, respectively. Energy gaps and lattice parameters obtained from HSE06 calculations are given in Table I, along with measured ones and those calculated using the LDA and GGA. Calculated energy gaps from the HSE06 functional range from 0.9 eV to 1.1 eV, consistent with previous findings [2,5,6, 8–10]. Further computational details are provided in Section III.

To study the thermal properties, harmonic and anharmonic interatomic force constants (IFCs) were computed from first principles. Harmonic IFCs were used to calculate phonon frequencies, ω_λ, and group velocities, v_λ, for mode $\lambda = (j, \mathbf{q})$ where j is the phonon branch and $\mathbf{q}$ its wave vector. Both sets of IFCs were used to calculate phonon-phonon scattering rates. The linearized Peierls-Boltzmann equation (PBE) was then solved using an iterative approach to obtain the non-equilibrium distribution function, $n_\lambda = n_\lambda^0 + (-\partial n_\lambda^0 / \partial T)\mathbf{F}_\lambda \cdot \nabla T$, resulting from a small temperature

gradient, ∇T. Here, n_λ^0 is the Bose distribution, and $(-\partial n_\lambda^0/\partial T)\mathbf{F}_\lambda \cdot \nabla T$ gives the deviation from equilibrium, where the vector, $\mathbf{F}_\lambda$, is determined iteratively from the recast PBE. Details of the iterative PBE solution have been provided in numerous previous references such as [20–24]. Using $\mathbf{F}_\lambda$, κ_{L} was calculated as:

$$\kappa_{\mathrm{L}}^{\alpha\beta} = \frac{1}{V}\sum_\lambda C_\lambda v_\lambda^\alpha F_\lambda^\beta, \tag{1}$$

where α and β are Cartesian components, V is the volume of the system and the mode specific heat is: $C_\lambda = k_B(n_\lambda^0+1)n_\lambda^0(\hbar\omega_\lambda/k_BT)^2$. We note that for the cubic (rock-salt) structures considered here, κ_{L} is a scalar.

A traditional measure of anharmonicity is provided by the mode averaged Grüneisen parameter, $\overline{\gamma}$ [25–27]. Below, we calculate $\overline{\gamma}$ to assess its utility in describing the anharmonicity in the three nitride compounds. It is given by:

$$\overline{\gamma} = \sum_\lambda C_\lambda \gamma_\lambda \Big/ \sum_\lambda C_\lambda. \tag{2}$$

In Eq. 2, γ_λ is the Grüneisen parameter for mode λ, given by the logarithmic derivative of the phonon frequencies with respect to volume, and it can be expressed in terms of the anharmonic IFCs as [28, 29]:

$$\begin{aligned}\gamma_\lambda &= -\frac{V}{\omega_\lambda}\frac{d\omega_\lambda}{dV} \\ &= -\frac{1}{6\omega_\lambda^2}\sum_\kappa\sum_{l'\kappa'}\sum_{l''\kappa''}\sum_{\alpha\beta\gamma}\Phi_{\alpha\beta\gamma}\left(0\kappa, l'\kappa', l''\kappa''\right)\frac{e_{\alpha\kappa}^{\lambda*}e_{\beta\kappa'}^{\lambda}}{\sqrt{M_\kappa M_{\kappa'}}}e^{i\mathbf{q}\cdot\mathbf{R}_{l'}}r_{l''\kappa''\gamma}.\end{aligned} \tag{3}$$

Here, $\Phi_{\alpha\beta\gamma}\left(0\kappa, l'\kappa', l''\kappa''\right)$ are the third-order anharmonic IFCs, $e^{\lambda}_{\alpha\kappa}$ is the α^{th} component of the phonon eigenvector for atom κ in mode λ, $\mathbf{R}_l$ is a lattice vector locating the l^{th} unit cell, κ specifies an atom in this cell whose mass is M_κ, and α, β and γ are Cartesian components. Finally, $r_{l\kappa\gamma}$ is the γ^{th} component of the vector locating the κ^{th} lattice atom in the l^{th} unit cell.

III Computation Method

DFT calculations were carried out in the plane wave basis as implemented in the Vienna Ab initio simulation package (VASP) [30–33] with the projector augmented wave (PAW) method [34]. The HSE06 band structures were obtained on an 8×8×8 **k** grid with the optimized lattice constants obtained from GGA calculations, discussed below. However, calculation of IFCs using the HSE06 functional would be prohibitively expensive. To circumvent this problem, we instead use the DFT+U formalism: The on-site interaction of the *d* electrons is treated within the rotationally invariant approach introduced by Dudarev et al. [35]. The rationale for choosing U is discussed below. For each U value, the lattice constant is optimized with a 12×12×12 **k** grid.

The harmonic IFCs were calculated with the help of Phonopy [36]. The harmonic IFCs can either be obtained by displacing the atoms from their equilibrium positions and calculating the forces, the finite displacement (FD) method, or by directly computing the Hessian matrix using density functional perturbation theory (DFPT) in VASP. In all calculations, we set the plane wave cutoff to 520 eV and the convergence in total energy to 10^{-8} eV. The harmonic IFCs were calculated on a 5×5×5 supercell made from the primitive cell, and containing 250 atoms. We have tested that the 2×2×2 **k** grid gives accurate phonon dispersions. For example, the phonon dispersions of ScN calculated from the 3×3×3 **k** grid are nearly identical to those obtained from the 2×2×2 **k** grid. We note that using Γ point sampling gave anomalous sensitivity of the phonon

dispersions on U, which was not found in the $2\times2\times2$ and $3\times3\times3$ cases. We have also compared the DFPT method and FD method and found that they gave practically the same phonon dispersions. In the following, we present phonon dispersions and thermal conductivity data with the harmonic IFCs from the DFPT method. The anharmonic IFCs were calculated with the FD method as detailed by Li et al. [24]. The forces were also computed on a 5×5×5 supercell but with the Γ point sampling. We consider IFCs up to the seventh nearest neighbors. This is equivalent to a distance cutoff of 1.42 a_0, where a_0 is the lattice constant. The PBE is then self-consistently solved for $\mathbf{F}_\lambda$ on a 48×48×48 **q** grid and the lattice thermal conductivity calculated according to Eq. (1). An adaptive Gaussian broadening scheme was used to account for the conservation of energy in the three-phonon scattering processes, where the broadening factor was set to unity [37, 38]. We have tested that the calculated thermal conductivities of the three nitride compounds are converged with respect to the supercell size in the harmonic IFC calculation and number of nearest neighbors in the anharmonic IFC calculation. We have also checked that the thermal conductivity is converged with regard to the **q** grid density and the broadening factor in the Gaussian scheme.

IV Results and Discussion

From Table I, it is seen that GGA and the hybrid functional HSE06 give lattice constants that are very close to the experiment values, while LDA underestimates the measured values by between 1 and 2%. However, standard DFT fails to correctly describe the electronic structure in these compounds. In the standard DFT calculations (GGA and LDA) ScN shows semi-metallic behavior, as has been found previously [7, 39]. For YN, GGA calculations give a semiconductor with an energy gap of about 0.2 eV, while calculations within LDA give a semimetal. For LuN,

only GGA and GGA+U calculations are performed since there are no LDA PAW potentials for Lu in VASP. Here, we find GGA predicts LuN to be a semiconductor with energy gap around 0.2 eV. Thus, for all compounds, the energy gaps obtained within DFT are too small. As noted above, other theoretical studies using more accurate treatment of exchange and correlation have shown that all of these compounds are semiconductors with sizable band gaps, consistent with the HSE06 calculations performed here.

The inputs to the transport calculation are the phonon modes and anharmonic phonon-phonon scattering rates, whose calculation requires the harmonic and anharmonic IFCs for each material. We have performed IFC calculations using DFT with on-site interactions for the *d* electrons accounted for using a Hubbard U. The challenge for this group of compounds is: what U to choose? One possibility is to choose the U value for each compound so as to match the measured lattice constants. We refer to this as Case 1. For this case, we find the calculated energy gaps to be smaller than those from the HSE06 hybrid functional calculations. This has been noted previously [2]. Alternatively, U could be chosen so that the energy gap matches that obtained from the HSE06 calculations. We call this Case 2. With increasing U, the *d* states become more localized, which reduces the bonding, causing the lattice constants to increase. For Case 2 they are too large compared to measured ones. Specifically, within LDA+U, choosing U values to match the energy gaps determined from the HSE06 calculations gives lattice constants that are 2% larger than the measured values for ScN and YN, respectively. GGA+U calculations give worse results: the lattice constants are 3% larger than the measured values for ScN, YN and LuN. For Case 1, lattice constants can be well-matched using LDA+U since LDA overbinds while increasing U increases the lattice constant. For the GGA calculations, the lattice constants are accurately reproduced with $U = 0$. However, as mentioned above, ScN is found to be

metallic. We note that DFT calculations for many semiconductors have accurately reproduced their phonon dispersions and thermal properties in spite of the fact that the calculated energy gaps were too small. Therefore, we focus below on Case 1, for which we perform LDA+U calculations for ScN, and YN, reserving GGA+U calculations only for LuN. Subsequently, we also examine Case 2, which allows us to compare the variation of the phonon dispersions and of κ_L values with U. A comparison of lattice constants, energy gaps and other quantities for the two cases is provided in Table II. A comparison of the band structures for the three compounds using DFT+U and HSE06 functional is given in Figs. S1 and S2 of the supplementary section [40].

Figure 2 shows the phonon dispersions calculated for different values of U: $U = 0$ (thin dotted black curves), Case 1 (thick solid red curves), and Case 2 (thin dashed blue curves). Note that all compounds show a large LO-TO splitting and softening of the TO mode at Γ. This is due in part to the large polarity of these compounds, reflected in their large Born effective charges (see Table II). Aside from decreasing the lattice constants and energy gaps, it is noted that decreasing the Hubbard U has almost no effect on the acoustic phonon branches, but increases LO-TO splitting through further softening of the TO branch.

The lattice thermal conductivity for the three compounds is plotted as a function of temperature for Case 1 in Fig. 3 (solid curves). ScN shows by far the highest κ_L of the three compounds, due to the relatively light Sc atom. The acoustic velocities are large, comparable to those in covalently bonded silicon: along the [100] direction they are 5730 m/s, 10008 m/s for TA and LA branches, respectively. By comparison, Si, which has about the same average atomic mass (28.08 for Si compared to 29.48 for ScN), has about the same TA velocity and 15% smaller LA velocity along [100]. However, the κ_L of ScN is almost three times smaller than that

of Si, which has κ_L about 140 $Wm^{-1}K^{-1}$ at 300 K [41–43]. This is primarily due to the larger phonon-phonon scattering rates, shown in Fig. 4.

It is interesting that LuN has almost the same κ_L as YN, despite the fact that the average atomic mass in YN is half that of LuN and the calculated acoustic velocities in YN are considerably larger: Along [100], v_{TA} = 4320 m/s, v_{LA} = 7735 m/s for YN, while v_{TA} = 3244 m/s, v_{LA} = 5625 m/s for LuN. Also, the LO-TO splittings for the two compounds are similar, as are the magnitudes of the anharmonic IFCs and mode averaged Grüneisen parameters (given below). The lower acoustic phonon velocities in LuN act to reduce κ_L. This is countered by a reduction in the phase space for phonon-phonon scattering, which gives larger phonon lifetimes and so acts to increase κ_L. To understand this latter behavior, we note that acoustic phonons carry almost all the heat in both YN and LuN. In a three-phonon scattering process, an acoustic phonon can scatter with (i) two other acoustic phonons (*aaa* process), (ii) one acoustic phonon and one optic phonon (*aao* process), or (iii) two optic phonons (*aoo* process). The contributions to the three-phonon scattering rates from these processes are plotted in Fig. 4 for the lowest acoustic (TA) phonon branch in ScN, YN, LuN and Si. Note that while the strength of *aaa* and *aoo* processes are similar in the three nitride compound, the *aao* processes in LuN remain much weaker than *aaa* and *aoo* processes over almost the full acoustic phonon frequency range. This is a direct consequence of the large frequency gap between acoustic and optic phonons, which exists in LuN except in a small region near the center of the Brillouin zone (see Fig. 2c, red curves). As a result, *aao* processes are severely restricted by momentum and energy conservation constraints. In contrast, in YN *aao* processes are as strong as *aaa* and *aoo* processes over about half of the

frequency range. The other two acoustic branches show qualitatively similar behavior. The result is smaller phonon lifetimes in YN compared to LuN.

The large LO-TO splittings in all three nitride compounds point to their having large static dielectric constants, ε_0. Values of ε_0 are calculated for all three materials using the Lyddane-Sachs-Teller relation: $\varepsilon_0 / \varepsilon_\infty = \omega_{\mathrm{LO}}^2 / \omega_{\mathrm{TO}}^2$ where ω_{TO} and ω_{LO} are the LO and TO phonon frequencies at Γ. Table II shows that all three nitride compounds have large ε_0. For Case 1, the values range from 37 for ScN to 84 for LuN. ε_0 for Case 2 is smaller than for Case 1 because of the smaller LO-TO splitting. We note that high values of ε_0 should contribute to efficient screening of ionized impurities in carrier transport.

To assess the sensitivity of the thermal conductivity to changes in U, we compare the temperature dependence of the κ_{L} values obtained for Case 1 (solid curves in Fig. 3) with those obtained for Case 2 (dashed curves in Fig. 3). Values at 300K are given in the last line in table II. The larger U values for Case 2 stiffen the TO branch frequencies around Γ, which reduces the phase space of energy and momentum conserving three-phonon scattering processes between heat carrying acoustic phonons and optic phonons. As a result, κ_{L} for Case 2 is larger than it is for Case 1. For ScN, the optic phonon branches hardly change going from Case 1 to Case 2 in spite of the large change in U from 2.6 eV to 7 eV. As a result, κ_{L} shows only modest increases (about 25% at 300K). For YN and LuN, the κ_{L} values increase a bit more than for ScN (33% and 35% respectively at 300K), reflecting somewhat larger shifts in the TO branches. The dependence of the κ_{L} as a function of U for YN is given in Fig. S3 and shows a roughly linear trend [40].

While it is computationally too expensive to perform phonon calculations using the HSE06 functional, we can nevertheless compare it to the DFT+*U* approach by examining the change in the energy per atom, ΔE, resulting from rigid shifts of the metal atom and N sublattices. Such shifts describe the TO phonon mode at Γ. A plot of ΔE as a function of the sublattice displacement, δ, is shown in Fig. 5 for ScN calculated using DFT+U with *U* for case 1 (gold curve) compared to that using the HSE06 functional (blue curve). For small δ, the two curves are almost identical. The TO frequencies extracted from these curves (using $\Delta E = \mu\omega_{TO}^2\delta^2/2$ where μ is the reduced atomic mass) are 10 THz for HSE06 and 11.3 THz for DFT+*U* (the TO frequency calculated from the first principles IFCs is 10.6 THz). The two values are in reasonable agreement suggesting that the DFT+*U* approach gives a good representation of the more accurate calculations. We note however that for materials near a structural transition, one should use caution since a dynamically stable structure obtained using DFT+*U* may be found to be unstable using HSE06 functional.

A conventional measure of κ_L is given from the theory of Liebfried and Schlömann (LS) [25], for which [26,27]: $\kappa_L = A\bar{M}\delta\omega_D^3 n^{1/3}/(\bar{\gamma}^2 T)$, where *A* is a constant, $\bar{M}$ is the average atomic mass, δ^3 is the volume per atom, ω_D is the acoustic Debye frequency (taken to be the highest acoustic phonon frequency), *n* is the number of atoms per unit cell, and $\bar{\gamma}$ is the mode averaged Grüneisen parameter. The expression has given reasonable predictions for many materials with zinc blende and rock-salt structures [26,27]. We have used this expression to compare the trends it predicts to the actual behavior determined from the *ab initio* calculations. We have calculated $\bar{\gamma}$ using Eqs. 2 and 3 for Case 1. While $\bar{\gamma}$ depends on temperature, *T*, it saturates at high *T*. By *T* = 300 K it is close to saturation for all materials, at which the calculated values are 1.66, 1.67

and 1.86 for ScN, YN and LuN, respectively. Then, using the lattice parameters from Table II and the ω_D values taken from the calculated phonon dispersions, we find that LS theory correctly predicts that ScN should have the highest κ_L. However, it predicts that the κ_L for LuN is much smaller than that of YN. In contrast, the first principles calculations predict that the κ_L for LuN and YN are similar (see Table II). The LS theory fails to capture behavior dictated by the interaction between acoustic and optic phonons, such as the smaller phase space for *aao* scattering responsible for the larger LuN κ_L. If the nitride compounds were weakly polar and did not have the soft TO modes such that the phonon dispersions had a large acoustic-optic frequency gaps, they would have much higher κ_L values.

To highlight this latter point, we first note that the masses of the TM and RE atoms in the three compounds studied here are all much larger than that of nitrogen, with mass ratios ranging from about 3 to over 12. It is then interesting to compare the κ_L values of these nitride compounds to those predicted for large mass ratio group IV and group III-V semiconductors, such as GaN, GeC, BSb, and BAs. It has been predicted from *ab initio* calculations that these four compounds should have room temperature κ_L values of 230$Wm^{-1}K^{-1}$, 480$Wm^{-1}K^{-1}$, 280 $Wm^{-1}K^{-1}$, and 2000$Wm^{-1}K^{-1}$. Upon isotopic enrichment of their heavy atoms, the calculated κ_L for GaN, BSb and GeC increase significantly to 400 $Wm^{-1}K^{-1}$, 1200 $Wm^{-1}K^{-1}$ and 1500 $Wm^{-1}K^{-1}$ [44–46], demonstrating the strong suppression of κ_L in large mass ratio compounds due to phonon-isotope scattering. We note that the TM and RE nitride compounds are either isotopically pure (ScN and YN), or have only small isotope concentrations on the heavy atom (La: 0.09% ^{138}La, 99.91% ^{139}La; Lu: 97.41% ^{175}Lu, 2.59% ^{176}Lu). Therefore, phonon scattering by isotopes is negligible compared to phonon-phonon scattering in these materials. The much

larger κ_L and enhancement with isotope enrichment in the group IV and III-V compounds arises primarily from large frequency gaps between acoustic and optic phonons (*a-o* gaps). Then, energy conservation in three-phonon processes sharply restricts scattering of heat-carrying acoustic phonons by optic phonons. Specifically, if the *a-o* gap is at least as large as the largest acoustic phonon frequency, then it is not possible to conserve energy in an *aao* scattering process, so such processes do not occur. Furthermore, energy conserving *aoo* processes can only occur for acoustic phonons whose frequency is smaller than the optic phonon bandwidth [47, 48]. For nonpolar or weakly polar crystals, such as the group IV and group III-V semiconductors, the bandwidth of the optic phonons is small, restricting *aoo* scattering to low frequencies only. The resulting weak phonon-phonon scattering makes κ_L quite sensitive to phonon scattering by isotopes. As is clear from the phonon dispersions, Fig. 2, the restrictions on both *aao* and *aoo* processes are not present in ScN, YN and LuN, soft TO phonon branch closes the *a-o* gap giving strong *aao* scattering, while the large optic phonon bandwidths promote strong *aoo* scattering.

Connected to the above, an interesting contrast to the TM and RE nitrides is boron bismuth (BBi). BBi crystallizes in the zinc blende structure [49], and electronic structure calculations using the YS-PBE0 hybrid functional have found this III-V compound to be semiconducting with an energy gap of 0.95 eV [50]. BBi has an extremely large heavy (Bi) to light (B) atom mass ratio of 19.3, much larger than that of LuN (12.5). We have calculated the phonon dispersions (see Fig. S4 [40]), the mode averaged Grüneisen parameter and the κ_L of BBi. It has smaller acoustic phonon group velocities than those in LuN, and the calculated $\overline{\gamma}$ at 300K is about 0.9, about half that of LuN. The BBi κ_L at 300K predicted from LS theory is slightly smaller than that of LuN. However, BBi is only weakly polar and the phonon dispersions show a large *a-o* gap of over 10 THz [49,50], which eliminates *aao* scattering and sharply restricts *aoo*

scattering. The temperature dependent κ_L of BBi calculated using the first principles approach is shown in Fig. 6; it is much larger than those of the three nitride compounds. The calculated room temperature κ_L is remarkably large, 347 $Wm^{-1}K^{-1}$, about 14 times that of LuN and far larger than predicted by the LS theory. We note that Bi is the heaviest isotopically pure element. The blue curve gives the κ_L for naturally occurring isotope mix on the B atom (19.9% ^{10}B, 80.1% ^{11}B). Isotopic purification of the B atoms (100% ^{11}B) gives only small increase in κ_L (red curve), a consequence of the light B mass and large Bi to B mass ratio.

Summary and Conclusions

The thermal properties of semiconducting ScN, YN and LuN, have been calculated from first principles. All three semiconductor compounds are highly polar. The soft TO modes contribute to suppressing the thermal conductivities, κ_L, because of strong scattering between acoustic (a) and optic (o) phonons. In contrast to the nitride compounds, the III-V semiconductor boron bismuth (BBi) has much larger κ_L (347 $Wm^{-1}K^{-1}$ at 300K) in spite of its larger Bi to B mass ratio and smaller acoustic velocities. The main difference responsible for the much larger κ_L in BBi is its weak polarity and has no soft TO modes, which creates a large a-o frequency gap that removes thermal resistance resulting from scattering between acoustic and optic phonons.

Synthesis of transition metal nitride compounds has been hampered by high N vacancy concentrations [1,51] resulting in part from low nitrogen vacancy formation energy. The resulting phonon-vacancy scattering may account for the measured κ_L in ScN [41] being much smaller than our calculated value. A similar reduction may occur in YN and LuN. This work demonstrates the utility of first principles calculations in describing thermal properties of materials. Furthermore, it highlights the importance of determining a physically reasonable value

of the Hubbard U parameter for calculations of thermal properties. Finally, it shows the importance of scattering between acoustic and optic phonons in reducing κ_L.

Acknowledgements

This research was supported primarily by the National Science Foundation under grant No. 1402949 (phonon dispersions, Grüneisen parameters and thermal conductivities), and also supported as part of the Solid-State Solar-Thermal Energy Conversion Center (S3TEC) an Energy Frontier Research Center funded by the U.S. Department of Energy (DOE), Office of Science, Basic Energy Sciences (BES), under Award # DE-SC0001299 / DE-FG02-09ER46577 (structure relaxation, electronic structure). The authors also acknowledge support from the Pleiades computational cluster at Boston College.

References

[1] F. Natali, B. J. Ruck, N. O. V. Plank, H. J. Trodahl, S. Granville, C. Meyer, and W. R. L. Lambrecht, Prog. Mater. Sci. **58**, 1316 (2013).

[2] X. Z. Yan, Y. M. Chen, X. Y. Kuang, and S. K. Xiang, J. Appl. Phys. **116**, 083707 (2014).

[3] B. Ul Haq, A. Afaq, G. Abdellatif, R. Ahmed, S. Naseem, and R. Khenata, Superlattices Microstruct. **85**, 24 (2015).

[4] G. Travaglini, F. Marabelli, R. Monnier, E. Kaldis, and P. Wachter, Phys. Rev. B **34**, 3876 (1986).

[5] D. Gall, M. Städele, K. Järrendahl, I. Petrov, P. Desjardins, R. T. Haasch, T.-Y. Lee, and J. E. Greene, Phys. Rev. B **63**, 125119 (2001).

[6] C. Stampfl, W. Mannstadt, R. Asahi, and A. J. Freeman, Phys. Rev. B **63**, 155106 (2001).

[7] W. A. Harrison and G. K. Straub, Phys. Rev. B **36**, 2695 (1987).

[8] M. Topsakal and R. M. Wentzcovitch, Comput. Mater. Sci. **95**, 263 (2014).

[9] B. Saha, J. Acharya, T. D. Sands, and U. V. Waghmare, J. Appl. Phys. **107**, 033715 (2010).

[10] B. Saha, T. D. Sands, and U. V. Waghmare, J. Appl. Phys. **109**, 073720 (2011).

[11] R. Deng, B. D. Ozsdolay, P. Y. Zheng, S. V. Khare, and D. Gall, Phys. Rev. B **91**, 045104 (2015).

[12] J. M. Ziman, *Electrons and Phonons* (Oxford University, London, 1960).

[13] J. Heyd, G. E. Scuseria, and M. Ernzerhof, J. Chem. Phys. **118**, 8207 (2003).

[14] D. Gall, I. Petrov, N. Hellgren, L. Hultman, J. E. Sundgren, and J. E. Greene, J. Appl. Phys. **84**, 6034 (1998).

[15] V. K. Becket and F. Ebert, Z. Für Phys. **31**, 268 (1925).

[16] L. Du, J. H. Edgar, R. A. Peascoe-Meisner, Y. Gong, S. Bakalova, and M. Kuball, J. Cryst. Growth **312**, 2896 (2010).

[17] C. P. Kempter, N. H. Krikorian, and J. C. McGuire, J. Phys. Chem. **61**, 1237 (1957).

[18] W. Klemm and G. Winkelmann, Z. Für Anorg. Allg. Chem. **288**, 87 (1956).

[19] T. Suehiro, N. Hirosaki, Y. Yamamoto, T. Nishimura, M. Mitomo, J. Takahashi, and H. Yamane, J. Mater. Res. **19**, 959 (2004).

[20] M. Omini and A. Sparavigna, Phys. B Condens. Matter **212**, 101 (1995).

[21] M. Omini and A. Sparavigna, Phys. Rev. B **53**, 9064 (1996).

[22] D. A. Broido, M. Malorny, G. Birner, N. Mingo, and D. A. Stewart, Appl. Phys. Lett. **91**, 231922 (2007).

[23] A. Ward, D. A. Broido, D. A. Stewart, and G. Deinzer, Phys. Rev. B **80**, 125203 (2009).

[24] W. Li, L. Lindsay, D. A. Broido, D. A. Stewart, and N. Mingo, Phys. Rev. B **86**, 174307 (2012).

[25] G. Leibfried and E. Schlömann, Nachr. Akad. Wiss. Göttingen II **a(4)**, 71 (1954).

[26] G. A. Slack, J. Phys. Chem. Solids **34**, 321 (1973).

[27] G. A. Slack, in *Solid State Phys.*, edited by H. Ehrenreich, F. Seitz, and D. Turnbull (Academic Press, 1979), pp. 1–71.

[28] J. Fabian and P. B. Allen, Phys. Rev. Lett. **79**, 1885 (1997).

[29] D. A. Broido, A. Ward, and N. Mingo, Phys. Rev. B **72**, 014308 (2005).

[30] G. Kresse and J. Furthmüller, Comput. Mater. Sci. **6**, 15 (1996).
[31] G. Kresse and D. Joubert, Phys. Rev. B **59**, 1758 (1999).
[32] G. Kresse and J. Furthmüller, Phys. Rev. B **54**, 11169 (1996).
[33] G. Kresse and J. Hafner, Phys. Rev. B **48**, 13115 (1993).
[34] P. E. Blöchl, Phys. Rev. B **50**, 17953 (1994).
[35] S. L. Dudarev, G. A. Botton, S. Y. Savrasov, C. J. Humphreys, and A. P. Sutton, Phys. Rev. B **57**, 1505 (1998).
[36] A. Togo and I. Tanaka, Scr. Mater. **108**, 1 (2015).
[37] W. Li, N. Mingo, L. Lindsay, D. A. Broido, D. A. Stewart, and N. A. Katcho, Phys. Rev. B **85**, 195436 (2012).
[38] W. Li, J. Carrete, N. A. Katcho, and N. Mingo, Comput. Phys. Commun. **185**, 1747 (2014).
[39] E. I. Isaev, S. I. Simak, I. A. Abrikosov, R. Ahuja, Y. K. Vekilov, M. I. Katsnelson, A. I. Lichtenstein, and B. Johansson, J. Appl. Phys. **101**, 123519 (2007).
[40] See Supplemental Material at http://... for ScN, YN and LuN band structure comparisons, YN thermal conductivities for different Hubbard U values and BBi phonon dispersions.
[41] We note that the κ_L of ScN thin films measured in Refs. 41 and 42 is considerably smaller than that calculated here. This may be due to the fact that ScN samples have large concentrations of defects.
[42] V. Rawat, Y. K. Koh, D. G. Cahill, and T. D. Sands, J. Appl. Phys. **105**, 024909 (2009).
[43] P. V. Burmistrova, J. Maassen, T. Favaloro, B. Saha, S. Salamat, Y. R. Koh, M. S. Lundstrom, A. Shakouri, and T. D. Sands, J. Appl. Phys. **113**, 153704 (2013).
[44] L. Lindsay, D. A. Broido, and T. L. Reinecke, Phys. Rev. Lett. **109**, 095901 (2012).
[45] L. Lindsay, D. A. Broido, and T. L. Reinecke, Phys. Rev. Lett. **111**, 025901 (2013).
[46] L. Lindsay, D. A. Broido, and T. L. Reinecke, Phys. Rev. B **88**, 144306 (2013).
[47] S. Lee, K. Esfarjani, T. Luo, J. Zhou, Z. Tian, and G. Chen, Nat. Commun. **5**, (2014).
[48] S. Mukhopadhyay, L. Lindsay, and D. S. Parker, Phys. Rev. B **93**, 224301 (2016).
[49] E. Deligoz, K. Colakoglu, Y. O. Ciftci, and H. Ozisik, Comput. Mater. Sci. **39**, 533 (2007).
[50] B. G. Yalcin, S. Bagci, M. Ustundag, and M. Aslan, Comput. Mater. Sci. **98**, 136 (2015).
[51] S. Kerdsongpanya, B. Alling, and P. Eklund, Phys. Rev. B **86**, 195140 (2012).

Table Captions

Table I Calculated and measured lattice constants and calculated energy gaps for ScN, YN and LuN.

Table II Lattice constants a, energy gaps E_g, Born effective charges Z^*, background and static dielectric constants ε_∞ and ε_0, and lattice thermal conductivities κ_L, for the on-site U values that give lattice constants matching the measured ones (left columns) and those that match the energy gaps from HSE06 calculations (right columns).

Table I

		ScN	YN	LuN
Lattice Constant (Å)	Experiment	4.501[a] 4.44[b]	4.881[c] 4.877[d]	4.76[e] 4.756[f]
	GGA	4.518	4.904	4.752
	LDA	4.437	4.821	NA
	HSE06	4.498	4.878	4.723
Energy Gap (eV)	GGA	0	0.20	0.24
	LDA	0	0	NA
	HSE06	0.92	1.10	1.14

[a]From Ref. 14,
[b]From Ref. 15,
[c]From Ref.16,
[d]From Ref. 17,
[e]From Ref. 18
[f]From Ref. 19

	ScN		YN		LuN	
U (eV)	2.6	7.0	2.0	5.6	0	4.2
a (Å)	4.500	4.594	4.883	4.988	4.752	4.893
E_g (eV)	0.2	0.93	0.40	1.10	0.24	1.12
Z*	4.05	3.51	4.30	3.59	4.52	3.64
ε_∞	11.05	7.83	11.46	7.47	12.48	7.52
ε_0	37.7	22.5	53.5	24.5	84.4	28.1
κ_L(W/mK)	51.5	64.5	24.8	33.1	27.3	36.8

Table II

Figure Captions

Figure 1 Electronic structure along high symmetry directions for (a) ScN, (b) YN, and (c) LuN, calculated using the HSE06 hybrid functional. Note that all three compounds have indirect energy gaps with valence band maxima at Γ and conduction band minima at X.

Figure 2 Phonon dispersions for (a) ScN, (b) YN, and (c), LuN for different values of the Hubbard U parameters: Black dotted curves are $U = 0$; red curves are Case 1, thin blue dashed curves are Case 2, as described in the text. Calculations for ScN and YN used LDA+U, while those for LuN used GGA+U.

Figure 3 Lattice thermal conductivity, κ_L, as a function of temperature for ScN, YN and LuN. The solid lines give κ_L for the U value that matches the measured lattice constant. Dashed curves give κ_L for the U value that matches the energy gap obtained from HSE06 hybrid functional calculations.

Figure 4 Contributions to three-phonon scattering rates of ScN, YN, LuN and Si in the lowest TA phonon branch from processes involving (a) three acoustic phonons (*aaa*), (b) two acoustic and one optic phonon (*aao*) and (c) one acoustic and two optic phonons (*aoo*), scaled by the maximum acoustic phonon frequency.

Figure 5 The change in energy per atom upon Sc and N sublattice displacements. The displacements are along the [100] direction with magnitudes prescribed by the corresponding phonon eigenvectors for the TO modes at Γ.

Figure 6 Lattice thermal conductivity of boron Bismuth (BBi) as a function of temperature. B has a mix of isotopes: 19.9% ^{10}B and 80.1% ^{11}B. The blue curve is calculated for this

isotope mix including phonon-isotope scattering, while the red curve assumes an isotopically purified case with 100% ^{11}B.

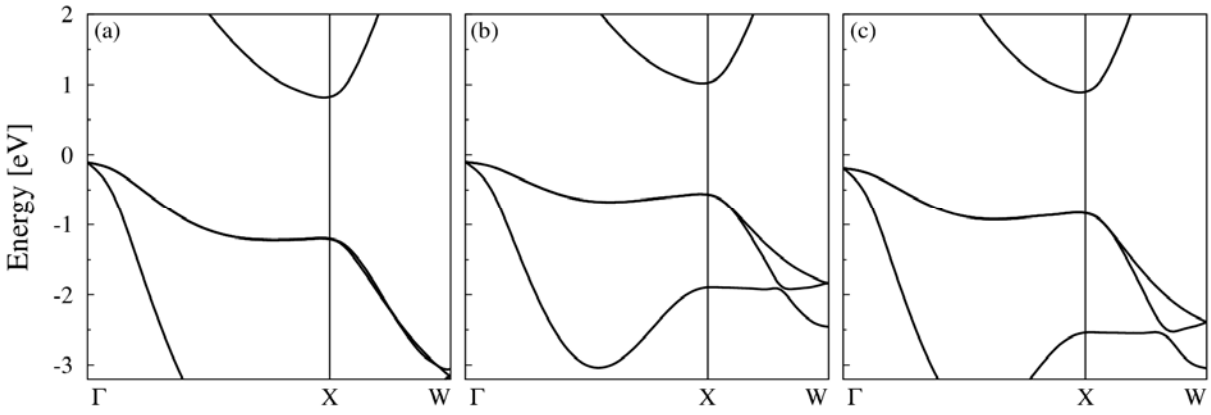

Figure 1

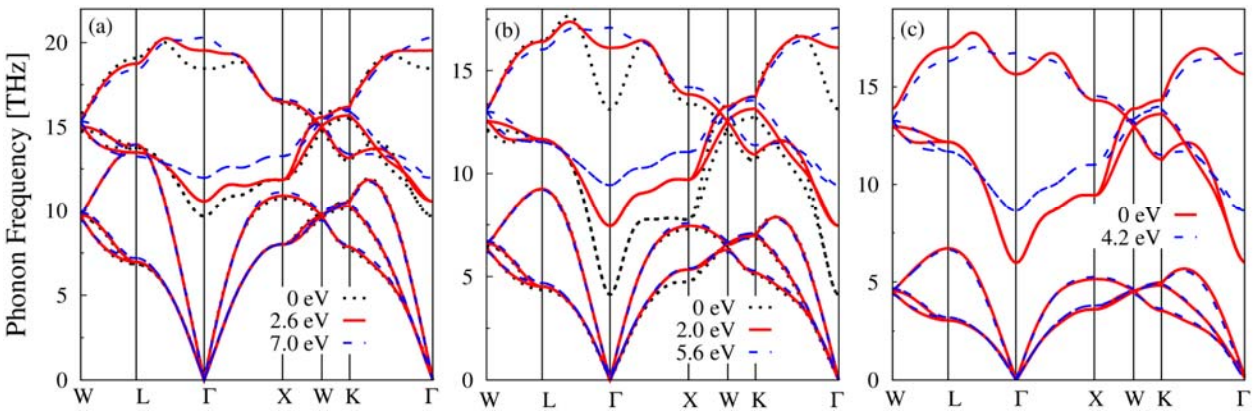
(a)
(b)
(c)
Phonon Frequency [THz]
0 eV
2.6 eV
7.0 eV
0 eV
2.0 eV
5.6 eV
0 eV
4.2 eV
W L Γ X W K Γ

Figure 2

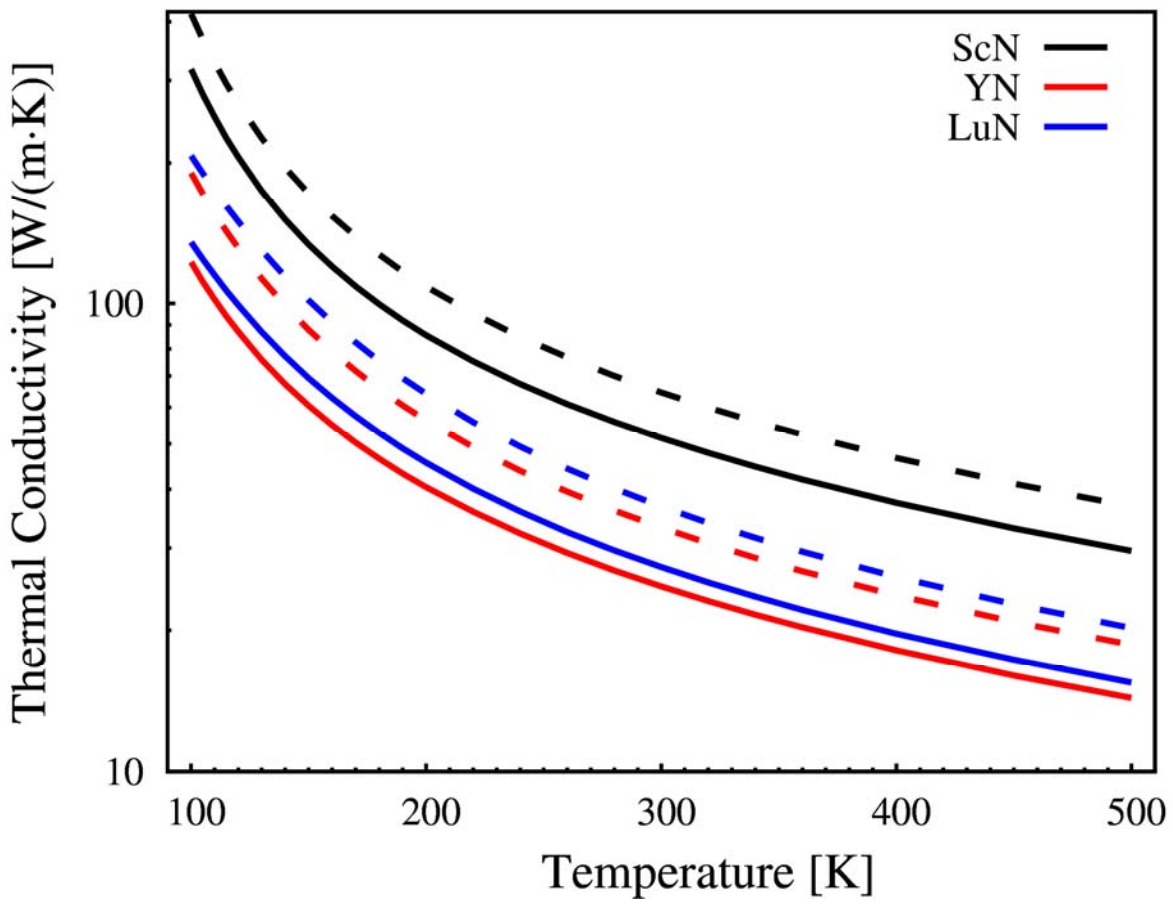
ScN
YN
LuN
Thermal Conductivity [W/(m·K)]
100
10
100
200
300
400
500
Temperature [K]

Figure 3

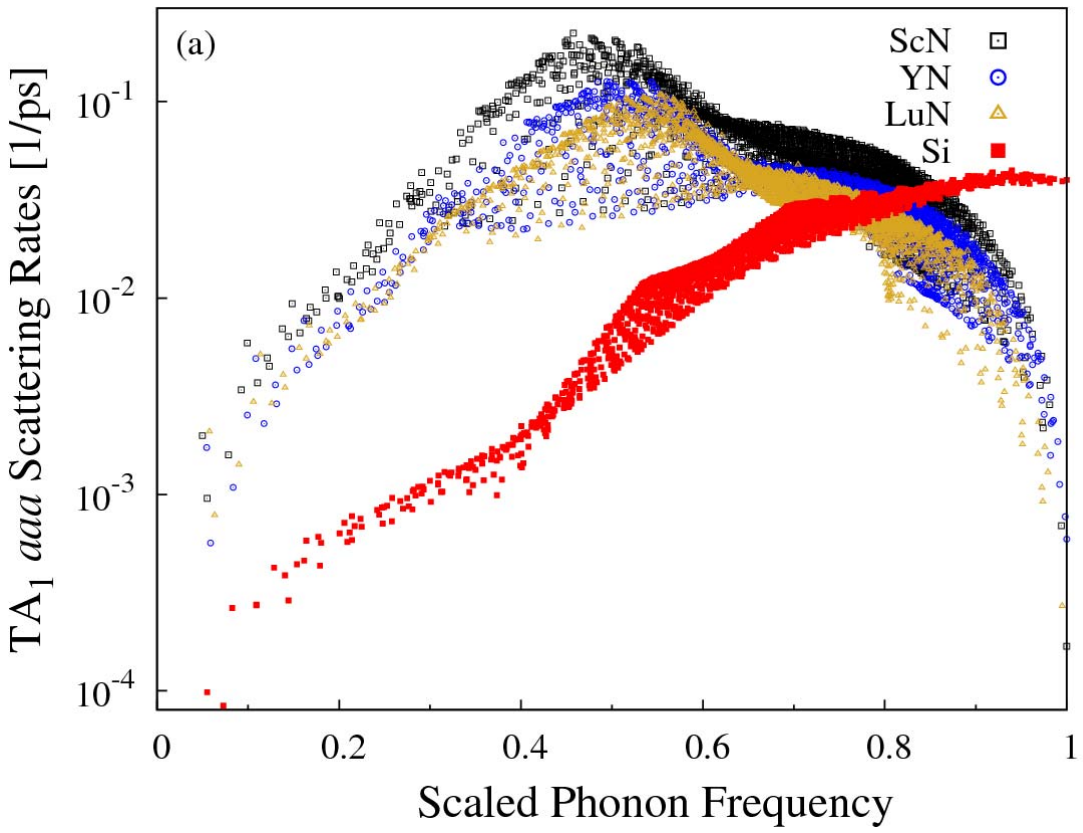
(a)
ScN
YN
LuN
Si
TA_1 *aaa* Scattering Rates [1/ps]
10^{-1}
10^{-2}
10^{-3}
10^{-4}
0
0.2
0.4
0.6
0.8
1
Scaled Phonon Frequency

Figure 4a

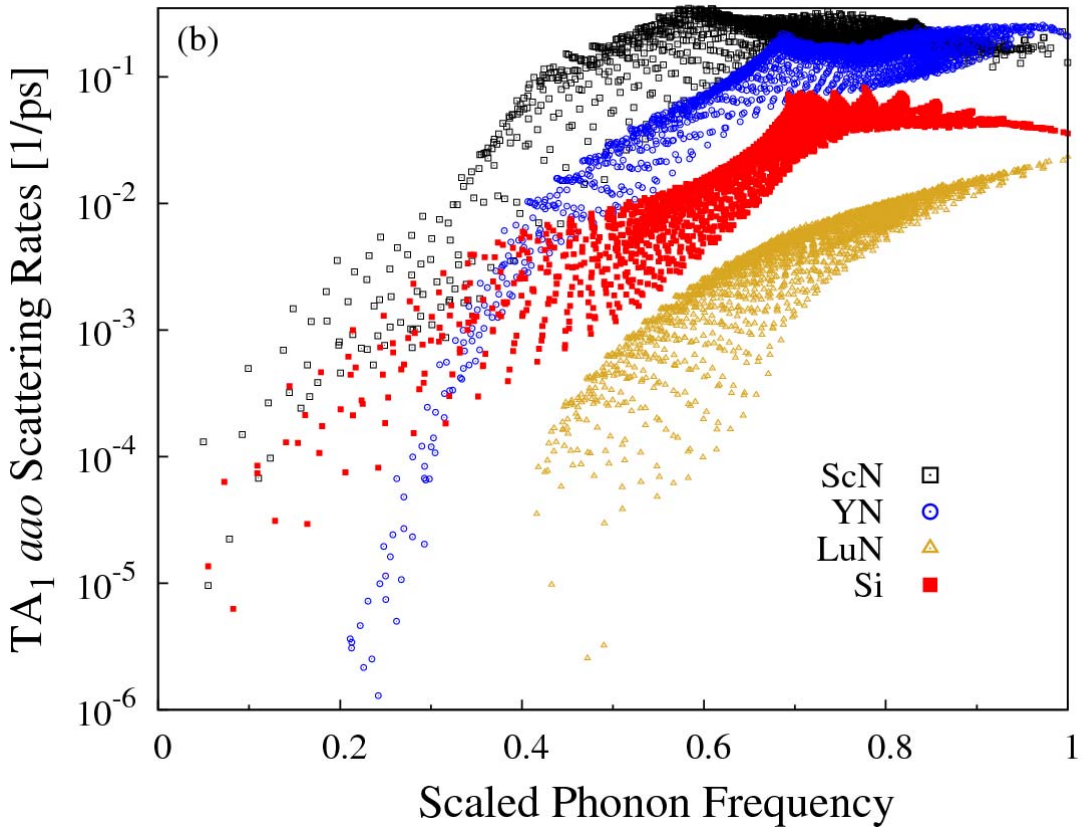
(b)
TA_1 *aao* Scattering Rates [1/ps]
10^{-1}
10^{-2}
10^{-3}
10^{-4}
10^{-5}
10^{-6}
0
0.2
0.4
0.6
0.8
1
Scaled Phonon Frequency
ScN
YN
LuN
Si

Figure 4b

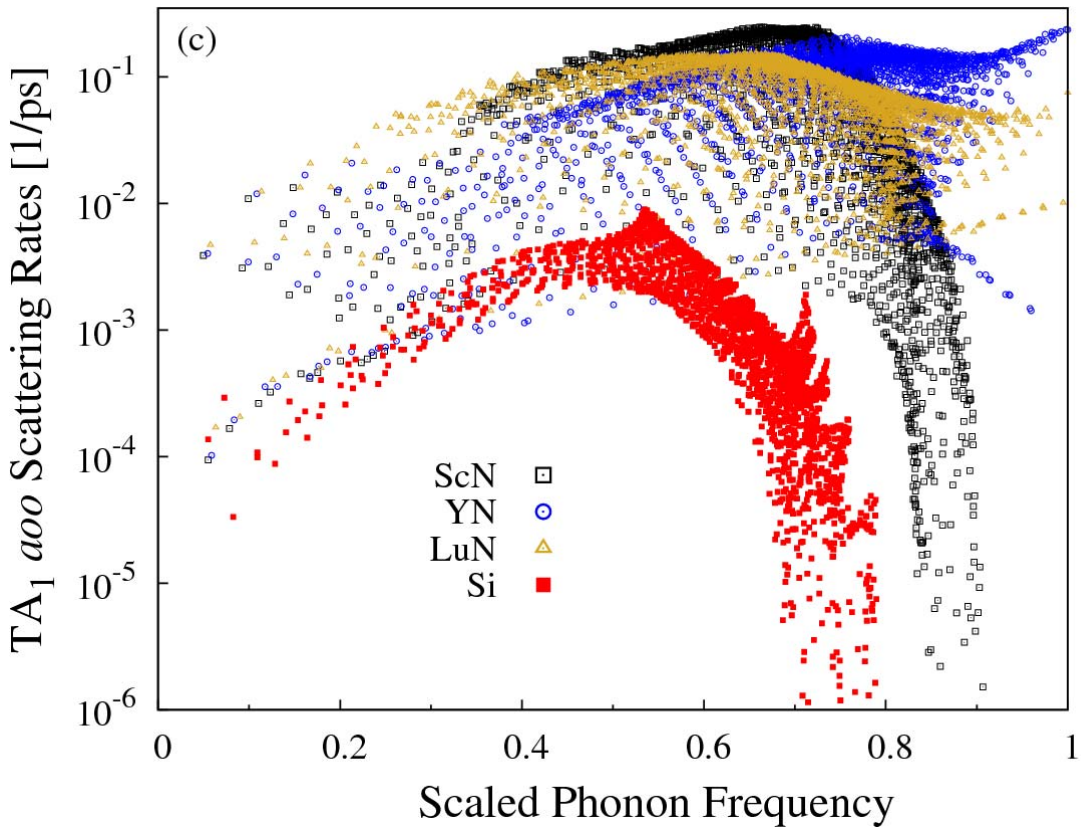
(c)
TA_1 *aoo* Scattering Rates [1/ps]
10^{-1}
10^{-2}
10^{-3}
10^{-4}
10^{-5}
10^{-6}
ScN
YN
LuN
Si
0
0.2
0.4
0.6
0.8
1
Scaled Phonon Frequency

Figure 4c

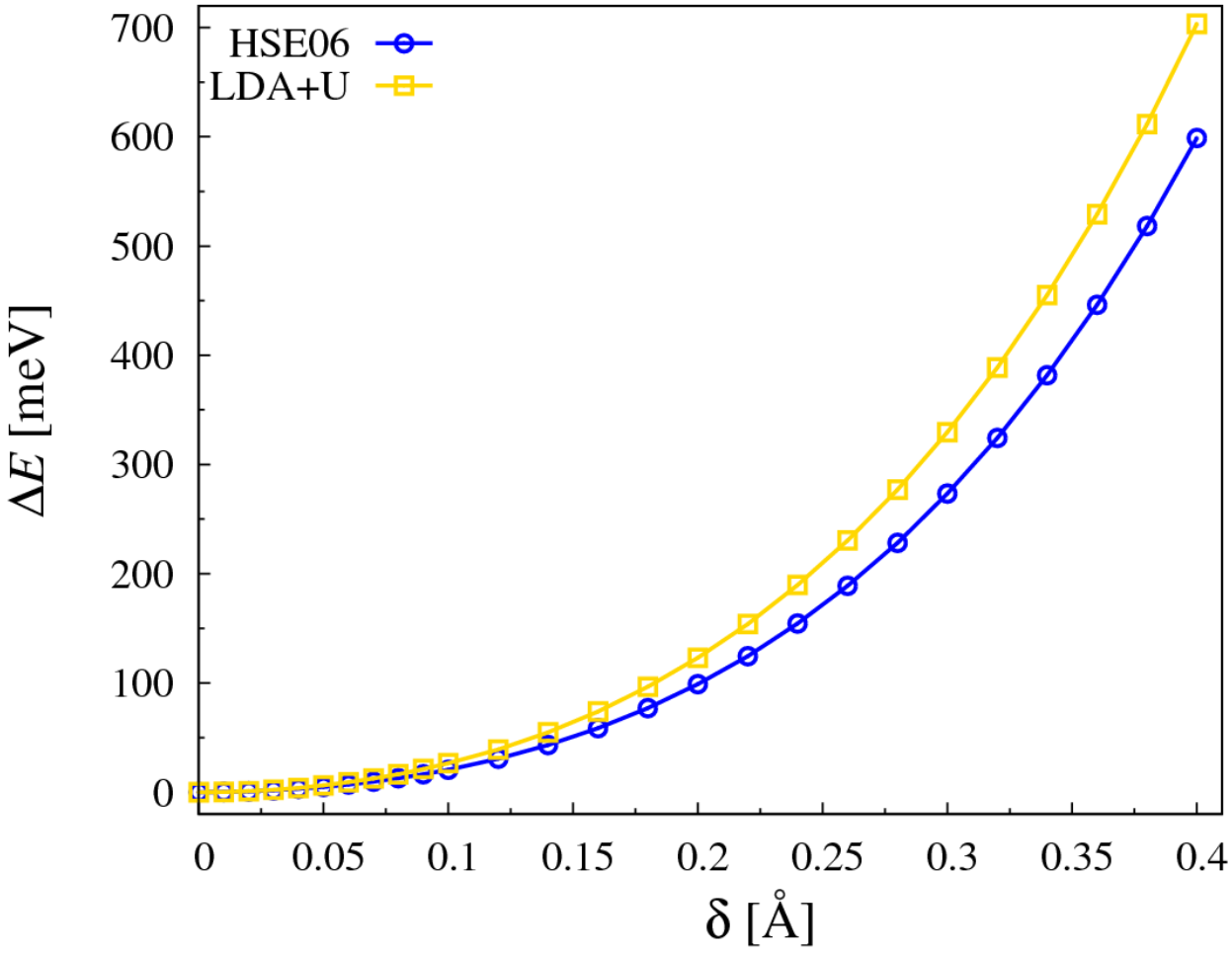
HSE06
LDA+U
700
600
500
400
300
200
100
0
ΔE [meV]
0
0.05
0.1
0.15
0.2
0.25
0.3
0.35
0.4
δ [Å]

Figure 5

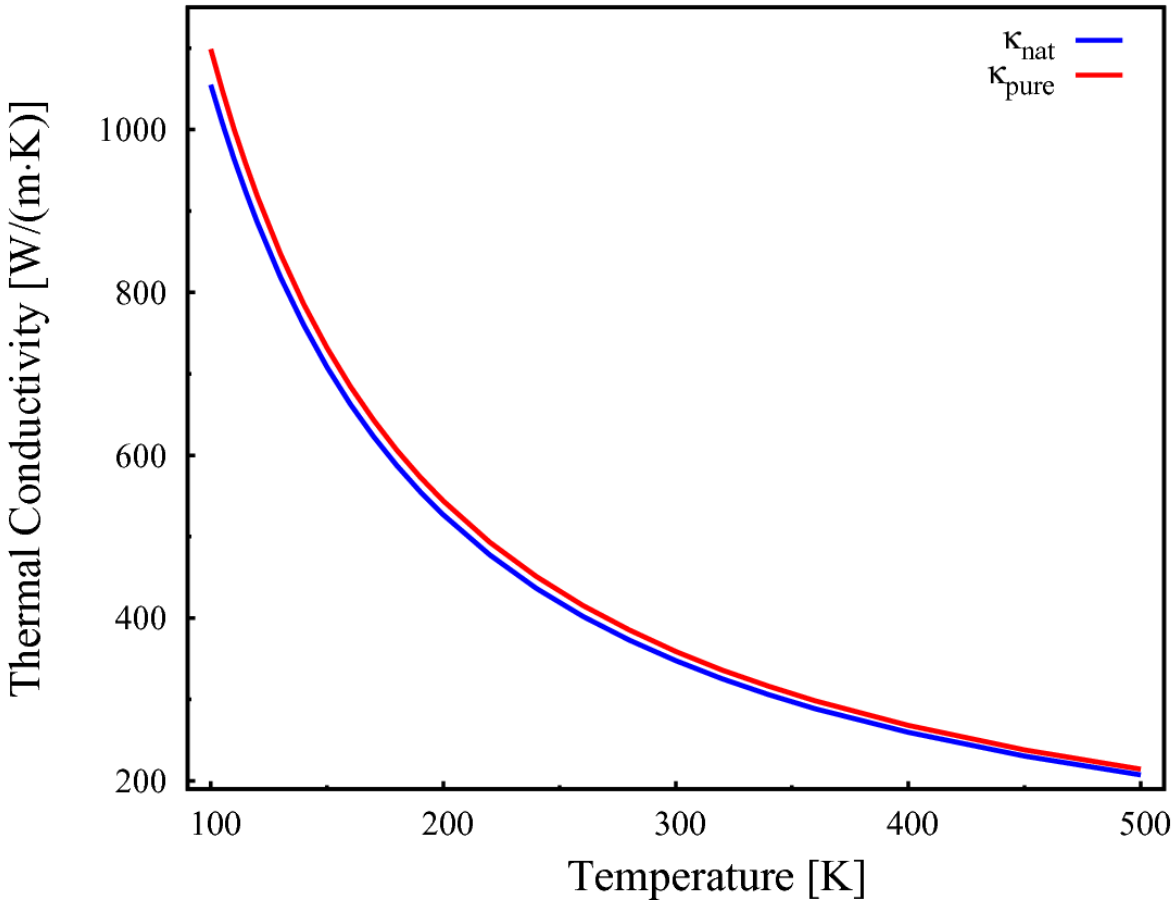
κnat
κpure
Thermal Conductivity [W/(m·K)]
1000
800
600
400
200
100
200
300
400
500
Temperature [K]
Figure 6